Int J Adv Manuf Technol (2016) 84:2547–2566
DOI 10.1007/s00170-015-7881-9

ORIGINAL ARTICLE

Process-parameter interactions in ultra-narrow gap laser welding of high strength steels

Wei Guo[1] · **Dave Crowther**[2] · **John A. Francis**[1] · **Alan Thompson**[2] · **Lin Li**[1]

Received: 27 October 2014 / Accepted: 21 September 2015 / Published online: 3 October 2015

Abstract S960 and S700 are two new high strength steels recently developed by Tata Steel, UK. Due to the high power densities that can be achieved, small component distortion, and fast welding speeds, laser welding of thick section steels has been widely used in offshore construction and shipbuilding. However, the penetration depth is typically limited in single pass welding to 1–2 mm/kW laser power. Melt sagging is a typical defect for single pass autogenous laser welding of thick section materials. Multi-pass narrow gap laser welding techniques become more attractive because they can weld thicker sections of material with a moderate laser power and suppress the melt sagging problem. In addition, this approach requires less filler material, and the cumulative heat input to the material is reduced when compared with traditional arc welding techniques. However, there are many variables involved in this narrow gap laser welding technique, which makes this process more complicated than single pass autogenous laser welding. In this study, the effects of multi-pass ultra-narrow gap laser welding parameter interactions (i.e. laser power, welding speed and wire feed rate) on laser weld quality and the welding efficiency for S960 high strength steel plates were investigated. Moderate laser powers of 1 to 2 kW were used to weld S960 high strength steel plates with a very narrow parallel groove (1.2 mm). Statistical design of experiments was carried out to assess the process parameter interactions and to optimise the ultra-narrow gap laser welding parameters. Validation experiments indicate that the proposed models predict the responses adequately within the range of welding parameters that were used. Defect-free welds in 6 mm thick S960 steel were obtained with only two passes, using the optimised welding parameters, and these optimised parameters were successfully transferred to the welding of 8 mm thick S960 steel. In addition, they were also successfully transferred to the welding of 13 mm thick S700 steel with a small modification. The optimised narrow gap laser welded joints show almost the same tensile properties as the base material, with failures occurring in the base material away from the weld.

Keywords High strength steel · Ultra-narrow parallel groove · Solid filler wire · Statistical modelling

1 Introduction

High strength steels are used in a wide variety of applications such as for structural components, pressure vessels and oil/gas transportation pipes, in shipbuilding, offshore construction (wind power and oil exploration) and in the automotive industry [1]. The application of high strength steels leads to not only to reductions in weight but also to compact structures [2]. Thin gauge high strength steels (0.8–3 mm thick and below) are widely used in the automotive industry [3–5]. For offshore pipelines, the current trends are towards the use of grade X70 steels with a wall thickness up to 40 mm, and for X80 and X100 pipeline steels with wall thicknesses of 25 mm and below [6].

Compared to traditional arc welding techniques, laser welding presents many advantages for the welding of high strength steels, such as rapid welding speeds, deeper penetration depths, narrower heat-affected zones and lower thermal distortions [7, 8]. However, there are limits to the maximum

✉ Wei Guo
wei.guo-2@manchester.ac.uk

[1] Laser Processing Research Centre, School of Mechanical, Aerospace and Civil Engineering, The University of Manchester, Sackville Street, Manchester M13 9PL, UK

[2] Tata Steel, Research & Development, Swinden Technology Centre, Moorgate, Rotherham, South Yorkshire S60 3AR, UK

laser power that is available in commercial lasers (typically less than 20 kW), which restricts the maximum welding depth using the single pass autogenous laser welding technique. It was reported that the laser penetration depth in single pass welding is typically in the order of 1–2 mm/kW [9, 10]. This will restrict the application of single pass laser welding to thick section components, such as thick offshore pipelines and pressure vessels. Autogenous laser welding (without a filler material) requires precise fit-up, which is often considered as a barrier to the wider applications of laser welding in the industry. In addition, thicker section laser welding with a single pass approach often results in porosity, molten material dropout, cracking and mis-tracking of weld seams [7, 11, 12].

Over the last few years, multi-pass narrow gap laser welding techniques have been demonstrated, which can be applied to the welding of very thick section components, using a filler wire and moderate laser powers. Zhang et al. [13] demonstrated that a 50-mm-thick 316L stainless steel plate could be welded using a narrow gap laser welding approach with a laser power of 8 kW and a groove width of 2–4 mm with a taper of 5°. In addition, the introduction of a filler wire into the welding groove can improve the metallurgy and the properties of the weld. These researchers effectively suppressed solidification cracks through controlling the chemical composition of the filler wire [13]. Elmesalamy et al. [14] successfully welded 316L stainless steel plates that were 20 mm in thickness using a 1-kW IPG single mode fiber laser with an ultra-narrow gap (1.5 mm gap width) and a taper of 3° from both sides using a multi-pass narrow gap laser welding technique. Li et al. [15] reported a combined approach which employed autogenous laser welding, laser welding with a filler wire and the hybrid laser-gas metal arc welding (GMAW) welding technique to weld a 30-mm-thick Q235 steel plate using a multi-layer, multi-pass process and a "Y" shaped groove.

Narrow gap laser welding is an emerging welding technique that can be applied to the welding of thick section materials with a narrow groove and a filler wire. However, this technique involves more complex process parameters when compared with autogenous laser welding as it has more interrelated variables. The relative distance between the laser beam and the filler wire, the laser power, the focal point, the angle between the wire and the laser beam, the welding speed, the filler wire diameter and the wire feed rate all have influences on the quality of the weld. All these variables make the narrow gap laser welding process more complicated than the single pass autogenous laser welding technique [16, 17]. The interactions between these welding parameters directly affect the quality of a welded joint. Traditionally, many welding trials with different welding parameters are carried out to optimise the welding parameters in order to obtain defect-free welded joints. This approach is inefficient, which leads to long process development times, consuming a large amount of test materials and energy.

Various statistical optimisation methods, such as response surface methodology (RSM), the Taguchi method and computational networks have been applied to defining the desired output variables through developing mathematical models that specify a relationship between the input parameters and output variables [18, 19]. In Benyounis and Olabi's [20] review of the application of these different statistical and numerical approaches, it was noted that RSM performs better than other techniques when a large number of experiments is not affordable. RSM is a statistical method that can be used to establish relationships between input variables and responses based on linear and quadratic polynomial equations. After the most important input variables have been identified, these equations can be optimised to span a reasonable range of process parameters [17, 20].

Elmesalamy et al. [9] used a statistical modelling approach to optimise the welding parameters for ultra-narrow gap laser welding of 316L stainless steel using a maximum laser power of 1 kW. In their work, the influences of laser power, welding speed and the wire feed rate on the integrity of the weld beads, the gap bridgability, the weld bead overlap factor, surface oxidation and the welding efficiency were investigated and optimised. Shi et al. [17] studied the interactions between welding parameters and the geometry of single beads using statistical methods. In their study, RSM based on a central composite design (CCD) was used and the validated models were applied to the multi-pass narrow gap laser welding of 20 mm thick AH32 high-strength ship steel. In order to obtain a reasonable range of geometric parameters for the single bead, the range in laser power was selected to be from 3 to 5 kW, while the range in welding speed was selected to be from 0.4 to 0.6 m/min, and the wire feed rate was selected to vary from 3 to 5 m/min. These workers successfully welded the 20-mm-thick high-strength ship steel plates after applying the models they created. However, some porosity and lack of fusion defects still existed in the weld beads.

As can be seen from the above discussion, statistical modelling is an effective approach for investigating multiple parameter interactions in narrow gap laser welding. However, no attempt has been made so far to assess the laser welding of S960 or S700 high strength steel plates using the narrow gap method. These two steels are relatively new, having only recently been developed by Tata Steel, UK. This study, therefore, aims to investigate process parameter interactions and study the influences of welding input parameters (laser power, welding speed and wire feed rate) on the three responses (i.e. integrity of the weld bead, the weld bead width and the number of filling passes) for the ultra-narrow gap laser welding of S960 high strength steel plates with thicknesses of 6 and 8 mm. The optimised welding parameters were also transferred to the welding of 13 mm thick S700 high strength steel plates. The tensile properties were examined in order to evaluate the quality of the optimised ultra-arrow gap laser welded high strength steel joints.

2 Experimental procedure

The materials used in this study were 6 and 8 mm thick S960 and 13 mm thick S700 high strength steel plates. S960 steel and S700 steel are both advanced high strength low alloy steels with minimum yield strengths of 960 and 700 MPa, respectively. Both steels were recently developed by Tata Steel (UK). These two steels are produced by thermo-mechanically controlled processing (TMCP) technology, which involves hot rolling of the steel at carefully controlled temperatures (i.e. controlled rolling) and/or quenching of the steel as part of the hot rolling process (i.e. direct quench). TMCP technology achieves a high strength with low levels of alloying through the exploitation of strengthening mechanisms such as precipitation hardening and/or grain refinement. The solid filler wires used for the welding of the S960 and S700 steels in this study were referred to as Union X96 (ER120S-G) with a diameter of 0.8 mm and Carbofil 2NiMoCr (ER120S-G) with a diameter of 1 mm, respectively. The chemical compositions for the steels and filler wires are given in Table 1, while the mechanical properties are shown in Table 2. All of these data were provided by Tata Steel, UK. The carbon equivalent (CE) values for the investigated steels and filler wires were calculated according to the IIW equation [21]:

$$CE = C + Mn/6 + (Cr + Mo + V)/5 + (Ni + Cu)/15 \quad (1)$$

A schematic diagram of the setup for the ultra-narrow gap laser welding process is given in Fig. 1. A continuous wave fiber laser (IPG YLS-16000) with a maximum achievable power of 16 kW was used in these experiments. The beam parameter product of the laser was 10 mm mrad and the beam was optically delivered (with a fiber core diameter of 300 μm) to the output lenses. The laser beam emitted from the end of the optical fiber was collimated with a lens with a 150-mm focal length and then focused onto the specimen surface using a lens with a 400-mm focal length. The measured focal spot size and Rayleigh length were 0.8 and 15 mm, respectively. The laser welding head was mounted on a six-axis KUKA robot. The filler wire was fed into the leading edge of the molten pool at an angle of 30° with respect to the specimen surface. Argon gas was blown onto the weld pool surface through a copper tube at a flow rate of 12 l/min, and the backing gas was delivered through a side tube to a shielding chamber under the specimen at a flow rate of 8 l/min to protect the back surface from oxidation.

Usually a "Vee" groove is prepared for narrow gap laser welding, and a filler wire is required in order to fill the groove using a multi-pass approach [13–15, 17]. However, the use of a Vee groove increases the volume of filler material that is consumed and the number of filling passes that is required. In the investigation of Yu et al. [22] on multi-pass narrow gap laser welding of 17 mm Q235 low-carbon steel plates, it was found that using a relatively small groove not only reduced the consumption of filler wire but it also reduced the deflection of the filler wire in the groove, which can improve fusion within the groove. So, in the present work, a parallel groove with a gap width of 1.2 mm was prepared for the S960 steel plates and a gap width of 1.4 mm was employed for the S700 steel plates. The groove geometries are shown in Fig. 2.

Prior to the welding experiments, the parent material in the vicinity of the machined groove was cleaned by sand blasting in order to remove the surface oxide, and it was then cleaned with ethanol. The welding trials for the design of experiments and statistical modelling stage, as well as for the process optimisation, were carried out on 6 mm thick S960 steel plates. The optimised welding parameters were then transferred to the welding of 8 mm thick S960 and 13 mm thick S700 steel plates. After welding, cross-sectional samples were extracted from the plates. The samples were ground and polished to a 1-μm finish, and then etched in a solution of 2 % Nital for

Table 1 Chemical compositions of base S960 and S700 steels, and Union X96 and Carbofil 2NiMoCr filler wires (wt%)

Material										
S960 steel	C	Mn	P	S	N	B	Ca	Si	Al	Cu
	0.088	1.51	0.008	0.002	0.0089	0.0022	0.012	0.055	0.033	0.014
	Sn	Cr	Ni	Mo	Ti	Nb	V	Fe	CE	
	0.001	0.472	0.023	0.248	0.025	0.040	0.050	Bal.	0.496	
Union X96	C	Si	Mn	Cr	Mo	Ni	Fe	CE		
	0.12	0.80	1.90	0.45	0.55	2.35	Bal.	0.793		
S700 steel	C	Mn	P	S	Si	Al	Cr	Mo	Nb	V
	0.068	1.476	0.009	0.001	0.05	0.073	0.495	0.19	0.03	0.044
	B	N	Fe	CE						
	0.0018	0.0045	Bal.	0.46						
Carbofil 2NiMoCr	C	Mn	Si	P	S	Cr	Ni	Mo	Fe	CE
	0.08	1.5	0.6	≤0.015	≤0.018	0.4	2.2	0.6	Bal.	0.68

Table 2 Mechanical properties of base S960 and S700 steels, and Union X96 and Carbofil 2NiMoCr filler wires

Material	Yield strength 0.2 % (MPa)	Tensile strength (MPa)	Elongation (%)	Impact value (J)
S960 steel	≥960	1000	7	120 (−40 °C)
Union X96	930	980	14	50 (−50 °C)
S700 steel	≥700	760	12	≥42 (−40 °C)
Carbofil 2NiMoCr	≥960	≥940	≥15	≥47 (−40 °C)

about 2 s. The assessment of the macrostructures for the welded joints was carried out using a KEYENCE VHX-500F optical microscope. Image analysis software (ImageJ) was applied to measure the weld bead widths and the cross-sectional areas of the welded samples. The microstructures of the welded joints and the distribution of alloying elements across the fusion zone were examined using a Zeiss EVO 50 scanning electron microscope (SEM) which was equipped with an energy dispersive X-ray detector (EDX).

Autogenous laser welding was used first to weld the 2-mm-thick root face. For root pass welding, a laser power of 2 kW was selected. The laser focal point was set 4 mm below the top surface of the specimen, i.e. the focal position coincided with the top surface of the landing at the weld root. The welding speed was varied from 20 mm/s (1.2 m/min) to 35 mm/s (2.1 m/min) in increments of 5 mm/s (0.3 m/min). Figure 3 shows the cross sections of the root pass welds at different welding speeds. It can be seen that all the root passes resulted in sound weld beads without defects. However, from the underside appearances of the root welds (see Fig. 4), it can be seen that there is discontinuous weld penetration with a welding speed of 35 mm/s (2.1 m/min). Full penetration was consistently achieved for welding speeds ranging from 20 mm/s (1.2 m/min) to 30 mm/s (1.8 m/min). However, the underside weld appearance was much smoother with a welding speed of 20 mm/s (1.2 m/min) when compared with 25 mm/s (1.5 m/min) and 30 mm/s (1.8 m/min). So welding parameters of 2 kW and 20 mm/s (1.2 m/min) were selected to weld the root face in the ultra-narrow gap laser welding experiments.

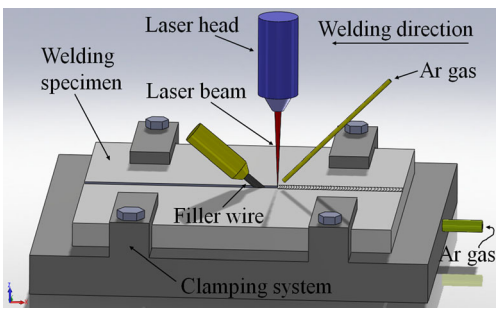

Fig. 1 Schematic representation of setup for ultra-narrow gap laser welding

After root pass welding, the laser beam was focused on the top surface of the specimens to perform the subsequent filling passes. A larger laser beam diameter at the beam/material interaction point in the groove would increase the coverage of the laser beam within the groove, which would be beneficial from the point of view of melting the filler wire and the groove walls in order to avoid lack of fusion during the filling passes.

Tensile test specimens for the as-received 8-mm-thick S960 and 13-mm-thick S700 base materials and the optimised welded samples were produced in accordance with ASTM E8M-04. Three replicates for tensile testing were prepared in each case to reduce experimental uncertainties. Samples prepared for tensile testing were extracted from the steady state region of the welds using wire electric discharge machining (EDM), with the long axis of each specimen type being normal to the welding direction. Tensile test coupons were sliced to coincide with the rolling direction of the material, and the configuration is shown in Fig. 5. The weld reinforcements in the face and root regions were removed by manual grinding before the tensile tests were conducted. Tensile tests were carried out on an Instron model 8500 electronic universal testing machine at room temperature.

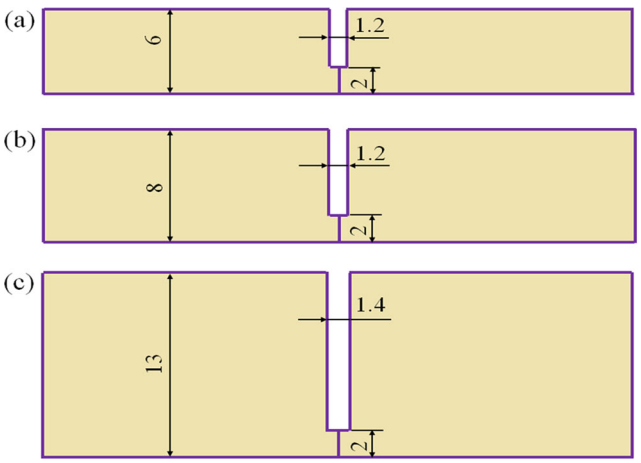

Fig. 2 Groove geometries for ultra-narrow gap laser welded specimens: **a** 6 mm thick S960 steel; **b** 8 mm thick S960 steel; and **c** 13 mm thick S700 steel

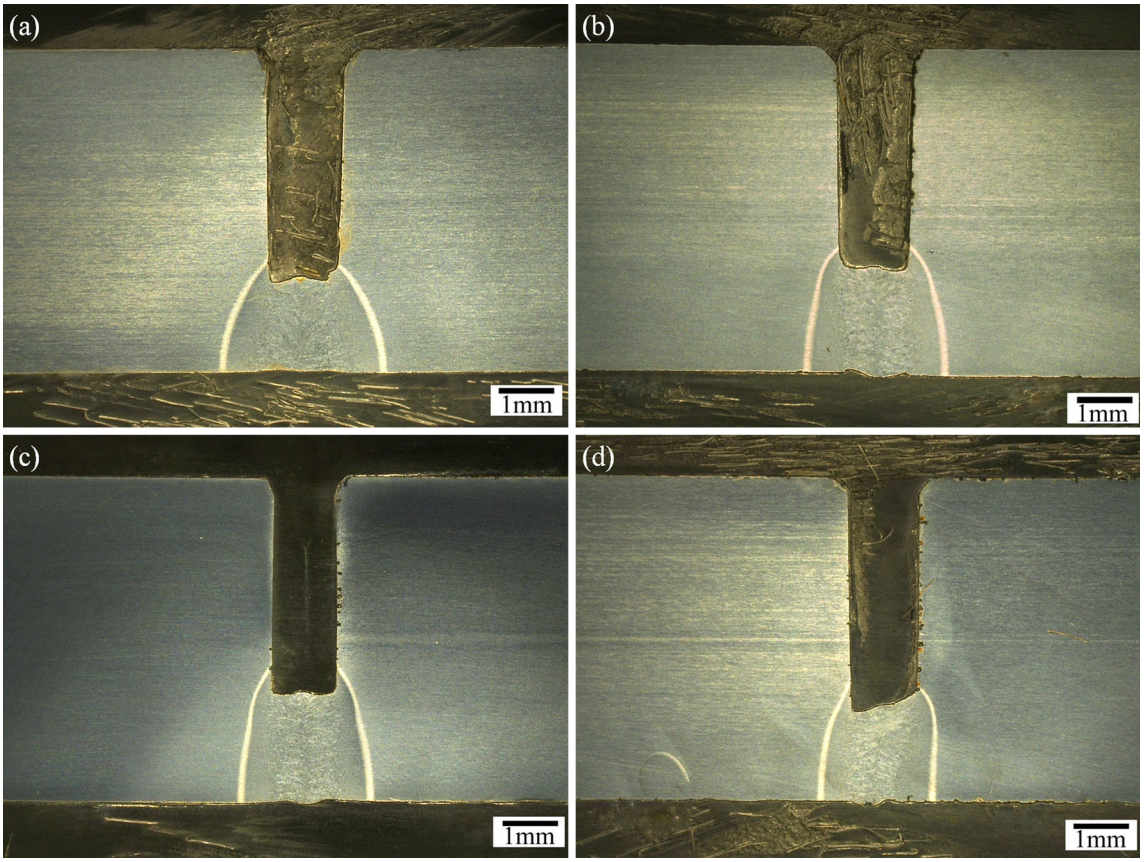

Fig. 3 Cross sections of the root pass welds for 6 mm thick S960 steel plates at different welding speeds: **a** 20 mm/s (1.2 m/min); **b** 25 mm/s (1.5 m/min); **c** 30 mm/s (1.8 m/min); and **d** 35 mm/s (2.1 m/min)

3 Design of experiments and statistical modelling approach

RSM is one of the most widespread statistical modelling approaches to identifying the significant processing parameters and quantifying their relationships with particular measured outputs [17, 23, 24]. The concept of RSM was introduced by Box and Wilson in 1951 [25]. RSM is a set of mathematical and statistical approaches that are useful for modelling and predicting one or more responses that are influenced by a number of input variables with the particular aim of optimising the responses [26, 27]. The functional relationship between a response of interest (Y) and input variables (x_i and x_j) can be illustrated by Eq. (2) [9, 24]:

$$Y = \alpha_0 + \sum_{i=1}^{k} \beta_i x_i + \sum_{i<j} \sum_{i=1}^{k} \beta_{ij} x_i x_j + \sum_{i=1}^{k} \beta_{ii} x_i^2 + \beta_0 \quad (2)$$

where α_0 is the random experimental error, β is a vector of p unknown coefficients, β_0 is the response at the centre point; β_i is the coefficient of the main linear components; β_{ij} is the coefficient of the two linear factor interactions, and β_{ii} is the coefficient of the quadratic factor.

The ultra-narrow gap laser welding technique involves several variable parameters, which affect the responses of interest and the optimum welding parameters. CCD is one of the most popular experiment designs, and it has been found to be most efficient in terms of the number of runs required [17, 24]. A CCD design consists of three types of design points (central, axial and factorial points) [9, 24].

Analysis of variance (ANOVA) can be used to determine the significant parameters and set the optimal level for each parameter, which is tested against regression. An F test was applied to each term in the model to check if the regression model was significant and to establish the significant model terms and their significance levels. The model terms are indicated as "significant" when values of "prob > F" are less than 0.05. In addition, the step-wise regression method was also applied to eliminate the insignificant model terms automatically. The "lack of fit value" represents the variation of actual data around the fitted model. If the "lack of fit" is not significant according to the F test results, this indicates that the model fits the data and this is desirable. The R^2 and the adjusted R^2 values are the other two criteria for assessing models. The R^2 parameter is used to indicate the adequacy

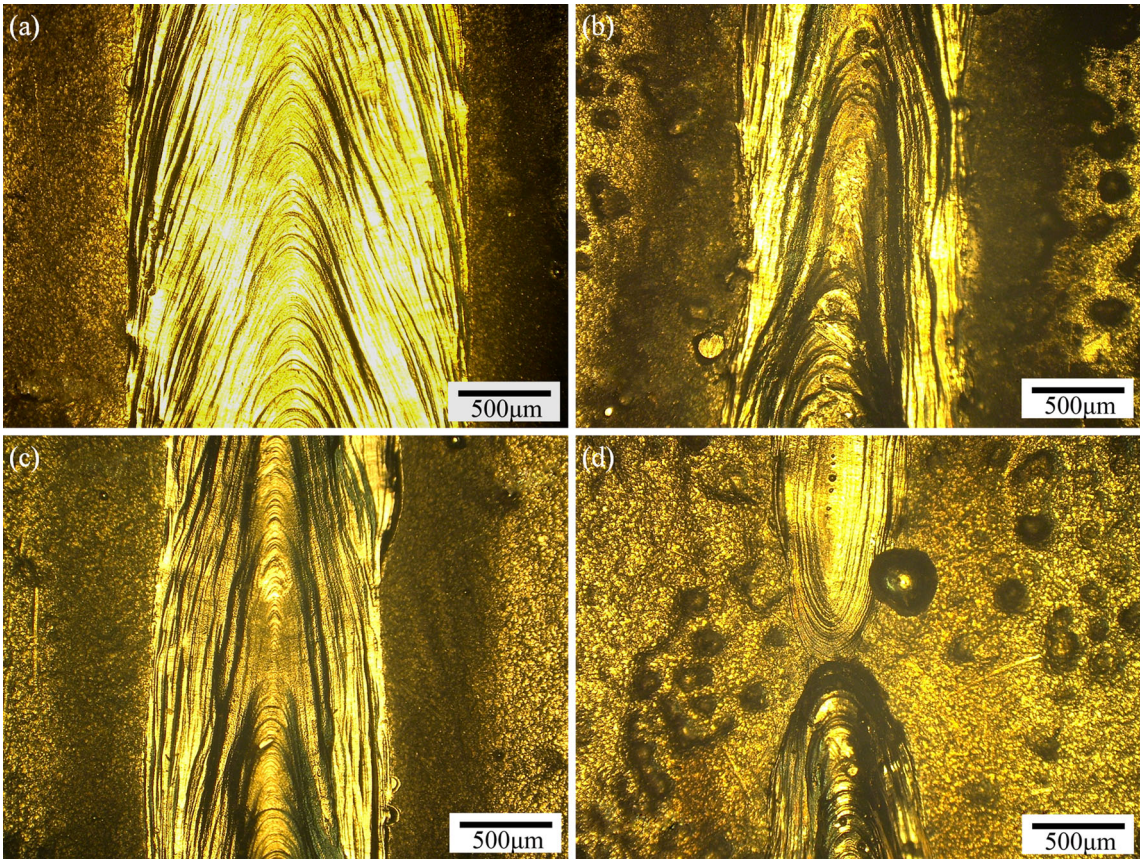

Fig. 4 Underside appearance of root welds at different welding speeds: **a** 20 mm/s (1.2 m/min); **b** 25 mm/s (1.5 m/min); **c** 30 mm/s (1.8 m/min); and **d** 35 mm/s (2.1 m/min)

of a fitted regression model [9, 28]. R^2 is a measure of the variation around the mean, and the adjusted R^2 value is a measure of the variation around the mean of the adjusted model terms. "R^2_{adj}" is calculated according to Eq. (3) [9]:

$$R^2_{adj} = \frac{n-1}{n-p} + \left(1-R^2\right) \tag{3}$$

where p is the number of model parameters and n is the number of experiments. Scatter diagrams were also used for regression. Perturbation curves and response surface graphs were derived for each model. "Adeq Precision" measures the signal-to noise ratio of each model. If the ratio is greater than 4, it indicates that the model is desirable [9, 17, 28, 29].

Based on the fit summaries, suitable response models for the response factors should be selected. In the work of Khan et al. on the optimisation of process parameters for the laser welding of martensitic stainless steels, two factor interaction (2FI) models were statistically recommended [30].

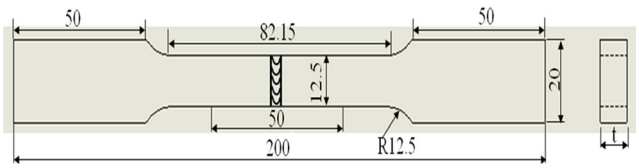

Fig. 5 Dimension and configuration of tensile test samples

In this investigation, a CCD experimental plan with three factors and five levels was used to implement the design matrix. The welding input variables were laser power, welding speed and wire feed rate. In order to find out the working range for each variable, preliminary bead-on-plate trials were carried out with a filler wire, by varying one of the process parameters at a time and checking the working ranges for acceptable weld quality. The integrity of the weld bead, the weld bead width and the number of filling passes were selected as the responses. The statistical modelling software package Design-Expert 7.0 was used to code the variables and to establish the design matrix. The independent process variables and factor levels, and the design matrix are shown in Tables 3 and 4, respectively. A set of 17 multi-pass ultra-narrow gap laser welding experiments was carried out with different welding parameters according to the design matrix. One sample was manufactured in the case of axial and factorial points, but the experiment for the central point was repeated three times.

Table 3 Independent variables and experimental design levels

Variable	Level 1 (−1)	Level 2 (−0.5)	Level 3 (0)	Level 4 (0.5)	Level 5 (1)
Laser power (kW)	1.0	1.2	1.5	1.8	2.0
Welding speed (mm/s)	10	13.6	19	24.4	28
Wire feed rate (mm/s)	10	19	33	46	55

4 Results and discussion

The experimental results for the weld bead integrity, the weld bead width and the number of filling passes are listed in Table 5. 2FI models were statistically selected for the responses: weld bead integrity, weld bead width and the number of filling passes. The measured responses were analysed using the Design-Expert 7.0 software. The weld bead integrity can be calculated according to [9]:

$$\text{Weld bead integrity} = \left(1 - \frac{\text{area of voids and lack of fusion}}{\text{total weld bead area}}\right) \times 100\% \quad (4)$$

The weld bead width was calculated according to the average width of each filling pass. The number of filling passes is the total number of filling passes required to fill the groove.

Typical macrographs from welded specimens made with different welding parameters are shown in Fig. 6. Examples of some typical weld defects are shown, for example, the wire failing to fill the groove completely (Fig. 6a). This can arise due to the wire getting caught in the weld groove, and the interruption to the filling process can lead to a large cavity in the groove. In sample 1 (Fig. 6a), this occurred in one of the early filling passes, and subsequent filling passes could not rectify the problem and fill the groove completely, leading to a low weld bead integrity. This also occurred in sample 2, as is evident in Table 5. Porosity and lack of side-wall fusion were also evident in some welds, as is highlighted in Fig. 6b.

On sample 10, an EDX linear scan across the final filling pass in the fusion zone was carried out. The SEM microstructure image and the location of the EDX linear scan are shown in Fig. 7a. The EDX linear scan results are shown in Fig. 7b. It can be seen that there are no clear variations in the concentrations of alloying elements across the fusion zone. This may because the concentrations of alloying elements in this steel and filler wire are very low.

4.1 Statistical models and analysis

4.1.1 Weld bead integrity model

The weld bead integrity is one of the most important factors to consider in assessing the quality of a weld. Good weld bead integrity often ensures that the mechanical properties (i.e. tensile strength, toughness, and fatigue properties) of an ultra-

Table 4 Design matrix with code independent process variables

Experiment no.	Point type	Factors		
		Laser power (kW)	Welding speed (mm/s)	Wire feed rate (mm/s)
1	Fact	1.0	28	10
2	Fact	2.0	28	10
3	Axial	1.5	19	46
4	Fact	2.0	10	10
5	Axial	1.2	19	33
6	Axial	1.5	13.6	33
7	Centre	1.5	19	33
8	Fact	2.0	28	55
9	Axial	1.5	19	19
10	Axial	1.8	19	33
11	Fact	2.0	10	55
12	Centre	1.5	19	33
13	Axial	1.5	24.4	33
14	Centre	1.5	19	33
15	Fact	1.0	10	10
16	Fact	1.0	10	55
17	Fact	1.0	28	55

Table 5 Experimentally measured responses

Experiment no.	Point type	Responses		
		Weld bead integrity (%)	Weld bead width (mm)	No. of passes
1	Fact	52	1.22	–
2	Fact	40	1.43	–
3	Axial	99.7	1.29	3
4	Fact	99.1	1.60	3
5	Axial	97.9	1.33	3
6	Axial	99.3	1.44	2
7	Centre	99.5	1.51	3
8	Fact	98.1	1.36	3
9	Axial	99.9	1.35	–
10	Axial	98	1.39	2
11	Fact	100	1.94	1
12	Centre	98.3	1.62	3
13	Axial	99.7	1.34	3
14	Centre	98.9	1.47	3
15	Fact	99.6	1.60	3
16	Fact	94.1	1.85	2
17	Fact	99.2	1.33	3

narrow gap laser welded joint are acceptable. In this investigation, the objective of this model was to maximise the weld bead integrity and thereby obtain a sound weld without defects (porosity and lack of fusion).

The ANOVA results for the weld bead integrity 2FI model are given in Table 6. An F value of 6.42 from the ANOVA results indicates that the model is significant. Values of prob > F less than 0.05 indicate that the model terms are significant, and vice versa. In this case, B (welding speed), C (wire feed rate) and the interaction of B and C (i.e. BC) are significant process parameters for the weld bead integrity model. The parameter A (laser power) as well as the interactions AB and AC are insignificant process parameters for the weld bead integrity model. These values represent adequate signals from the model, and they can be used to navigate the whole design space. Model validation measures are given as R^2=0.7938 and adjusted R^2=0.6701. The adequate precision measures the signal-to-noise ratio. The value of 8.773 is greater than 4 and it indicates an adequate signal.

From the above analysis, the final mathematical model for the weld bead integrity in terms of coded factors as derived by the design expert software package is as shown below:

$$\begin{aligned}\text{Weld bead integrity} = {} & 92.55 - 0.88 \times \text{A} - 11.84 \times \text{B} \\ & + 11.53 \times \text{C} - 2.31 \times \text{A} \times \text{B} \\ & + 2.16 \times \text{A} \times \text{C} + 13.74 \times \text{B} \times \text{C}\end{aligned} \quad (5)$$

4.1.2 Weld bead width model

The width of the weld bead is another important factor in assessing the quality of the weld. It demonstrates the ability of the filler wire to fill the prepared groove without lack of fusion. The wider the weld bead is, the better the mixing of the filler wire and the base material will be, but if the weld bead is too wide, then more energy will be required per unit length of weld and the productivity will drop. A suitable width for the weld bead will ensure that the laser energy is used effectively and it will assist in ensuring that a sound welded joint with satisfactory mechanical properties will be obtained. In this investigation, the objective of this model was to achieve a weld bead width that exceeded the width of the weld groove by a specified amount, thereby producing a sound weld without lack of fusion.

The results of ANOVA are given in Table 7. The F value of 4.09 implies that the model is significant. Values of prob>F less than 0.05 indicate that the model terms are significant. In this case, B (welding speed) is a significant model term. A (laser power), C (wire feed rate), and the interactions AB, AC and BC are insignificant model terms for the weld bead width model. The "lack of fit F value" of 3.41 implies that the lack of fit is not significant relative to the pure error. These values would suggest that we have adequate signals from the model, and that they can be used to navigate the whole design space. Model validation measures are given as R^2=0.7104 and adjusted R^2=0.5366. The adequate precision measures the signal-to-noise ratio. The value of 7.185 is greater than 4 and it indicates an adequate signal.

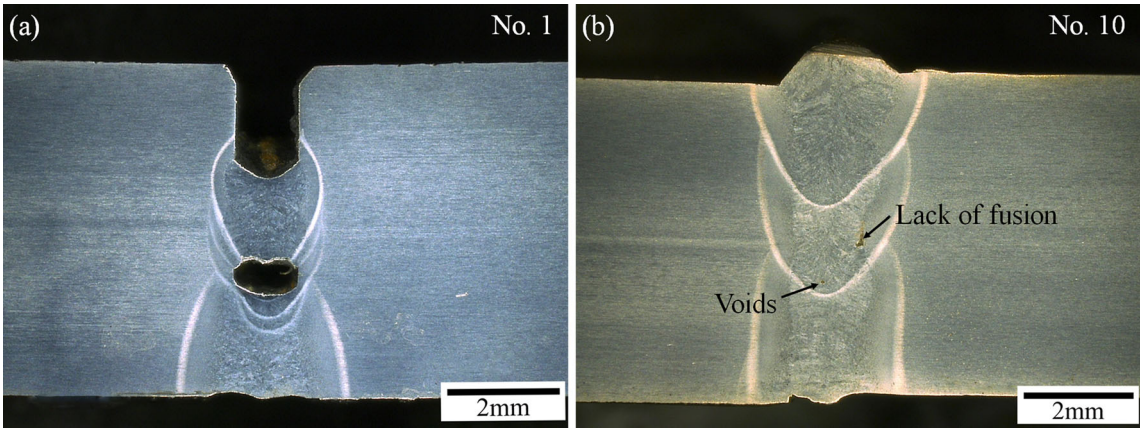

Fig. 6 Selected macrographs showing the bead shape, bead width, the number of passes and some typical defects. The *number* on each macrograph indicates the sample number

From the above analysis, the final mathematical model in terms of coded factors as derived by the design expert software package is as given below:

$$\begin{aligned}\text{Bead width} = {} & 1.47 + 0.042 \times \text{A} - 0.20 \times \text{B} \\ & + 0.068 \times \text{C} + 0.019 \times \text{A} \\ & \times \text{B} - 0.011 \times \text{A} \times \text{C} - 0.069 \times \text{B} \\ & \times \text{C} \end{aligned} \quad (6)$$

4.1.3 Number of filling passes model

The number of filling passes embodies the efficiency with which the filler wire fills the groove in ultra-narrow gap laser welding. Experimental results indicate that different numbers of filling passes are required to fill the ultra-narrow groove completely with different combinations of welding parameters. It is known amongst welding practitioners that the preparation work prior to welding is much more time-consuming than the welding process itself, and also that the interactions among the welding parameters are complex. However, an increase in the number of filling passes that is needed to fill the groove will increase the probability of generating welding defects such as porosity and lack of fusion in the weld. In addition, a higher number of filling passes implies a low filling efficiency for an individual filling pass, which will increase the cumulative heat input to the specimen. More welding passes could also result in a larger butterfly distortion of the weld, which will increase the possibility of the filler wire failing to fill in the groove completely due to problems with access. In this investigation, the objective of this model was to minimise the number of filling passes while achieving a high welding efficiency.

ANOVA of the number of filling passes reduced 2FI model (Table 8) gives the results of analysis of variance. The F value of 6.05 implies that the model is significant. Values of prob>F less than 0.05 indicate that the model terms are significant. In this case, B (welding speed) is a significant model term. A

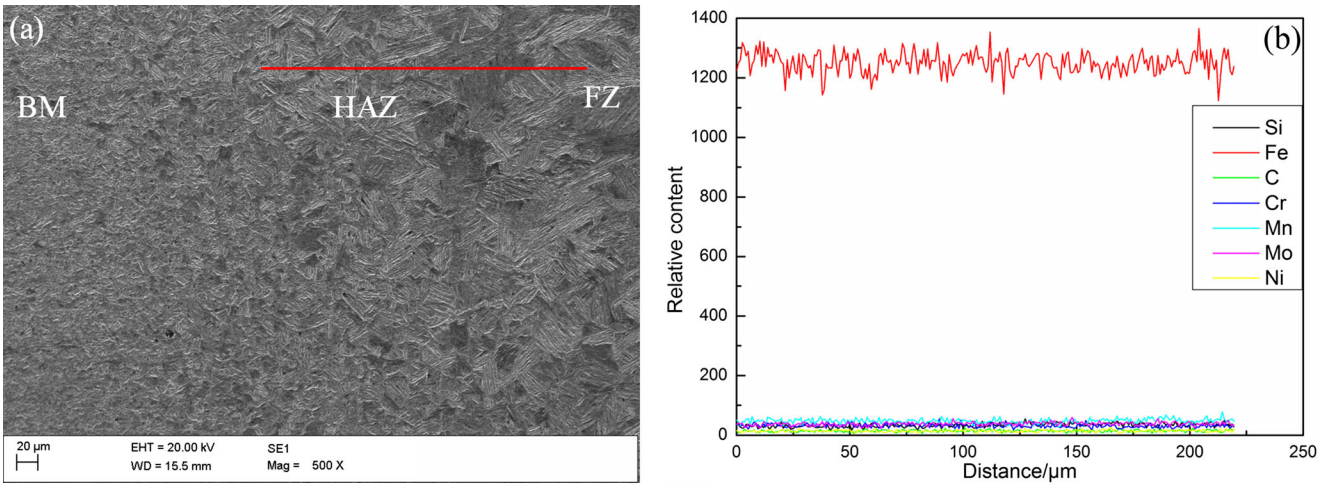

Fig. 7 SEM microstructure image and EDX linear scan results for NGLW in S960 steel: **a** SEM microstructure image highlighting location of EDX linear scan; **b** EDX linear scan results across the last filling pass in the fusion zone of sample 10

Table 6 ANOVA table for weld bead integrity 2FI model

Source	Sum of squares	df	Mean square	*F* value	*p* value Prob>*F*	
Model	3979.55	6	663.26	6.42	0.0054	Significant
A-power	6.69	1	6.69	0.065	0.8043	
B-welding speed	1222.78	1	1222.78	11.83	0.0063	
C-wire feed rate	1160.13	1	1160.13	11.22	0.0074	
AB	42.78	1	42.78	0.41	0.5345	
AC	37.41	1	37.41	0.36	0.5608	
BC	1509.75	1	1509.75	14.61	0.0034	
Residual	1033.64	10	103.36			
Lack of fit	1032.92	8	129.11	358.65	0.0028	Significant
Pure error	0.72	2	0.36			
Cor total	5013.18	16				

(laser power), C (wire feed rate) and the interaction BC are insignificant model terms for the number of filling passes model. These values suggest that we have adequate signals from the model, and they can be used to navigate the whole design space. Model validation measures are given as R^2= 0.7288 and adjusted R^2=0.6083. The adequate precision measures the signal-to-noise ratio. The value of 8.567 is greater than 4 and it indicates an adequate signal.

From the above analysis, the final mathematical model in terms of coded factors as derived by the design expert software package is as given below:

$$\text{number of passes} = 2.77 - 0.24 \times \text{A} + 0.54 \times \text{B} - 0.47 \times \text{C} + 0.24 \times \text{B} \times \text{C} \quad (7)$$

4.2 Diagnostics of the models

The normality of the residual data is normally checked in order to validate the statistical models. The residuals (the deviations between the predicted and actual values of responses) should follow a normal distribution with a mean value of 0. The method of least squares is usually employed in regression analysis. In an ideal scenario, a straight line is produced, which indicates no abnormalities [17, 31]. Figure 8 shows the normal plots of residuals for the weld bead integrity, the weld bead width and the number of filling passes. It can be seen that most of the points are located on the straight line or close to the straight line, except for a limited number individual points, which indicates that the models are effective.

4.3 Validation of the models

The fitted values are plotted of against measured values for the weld bead integrity model, the weld bead width model and the number of filling passes model in Fig. 9a–c, respectively. The measured values fall close to the diagonal line in most cases, which suggests that good fits to the data have been achieved. These comparisons in combination with those presented in Fig. 8 indicate that the models are well behaved.

Table 7 ANOVA table for the weld bead width 2FI model

Source	Sum of squares	df	Mean square	*F* value	*p* value Prob>*F*	
Model	0.43	6	0.072	4.09	0.0247	Significant
A-power	0.015	1	0.015	0.87	0.3727	
B-welding speed	0.34	1	0.34	19.01	0.0014	
C-wire feed rate	0.040	1	0.040	2.29	0.1609	
AB	2.812E−003	1	2.812E−003	0.16	0.6981	
AC	1.012E−003	1	1.012E−003	0.057	0.8155	
BC	0.038	1	0.038	2.14	0.1739	
Residual	0.18	10	0.018			
Lack of fit	0.16	8	0.021	3.41	0.2468	Not significant
Pure error	0.012	2	6.033E−003			
Cor total	0.61	16				

Table 8 ANOVA table for the number of filling passes reduced 2FI model

Source	Sum of squares	df	Mean square	*F* value	*p* value Prob>*F*	
Model	3.8	4	0.95	6.05	0.0121	Significant
A-power	0.38	1	0.38	2.42	0.1539	
B-welding speed	0.95	1	0.95	6.03	0.0364	
C-wire feed rate	0.65	1	0.65	4.14	0.0725	
BC	0.16	1	0.16	1.02	0.3382	
Residual	1.41	9	0.16			
Lack of fit	1.41	7	0.20			
Pure error	0	2	0			
Cor total	5.21	13				

4.4 Effects of welding parameters on the responses

4.4.1 Effects of welding parameters on weld bead integrity

The perturbation plot for the effects of welding parameters on the weld bead integrity is shown in Fig. 10. The welding speed and the laser power have an inverse correlation with the integrity of the weld bead. At higher welding speeds, the weld bead integrity reduces significantly. This may be because a fast welding speed results in a fast cooling rate. Pores may not have sufficient time to escape from the molten pool. In addition, the molten filler wire does not have sufficient time to fill the groove well before it solidifies, which may lead to some lack of fusion in the weld. The laser power has only a

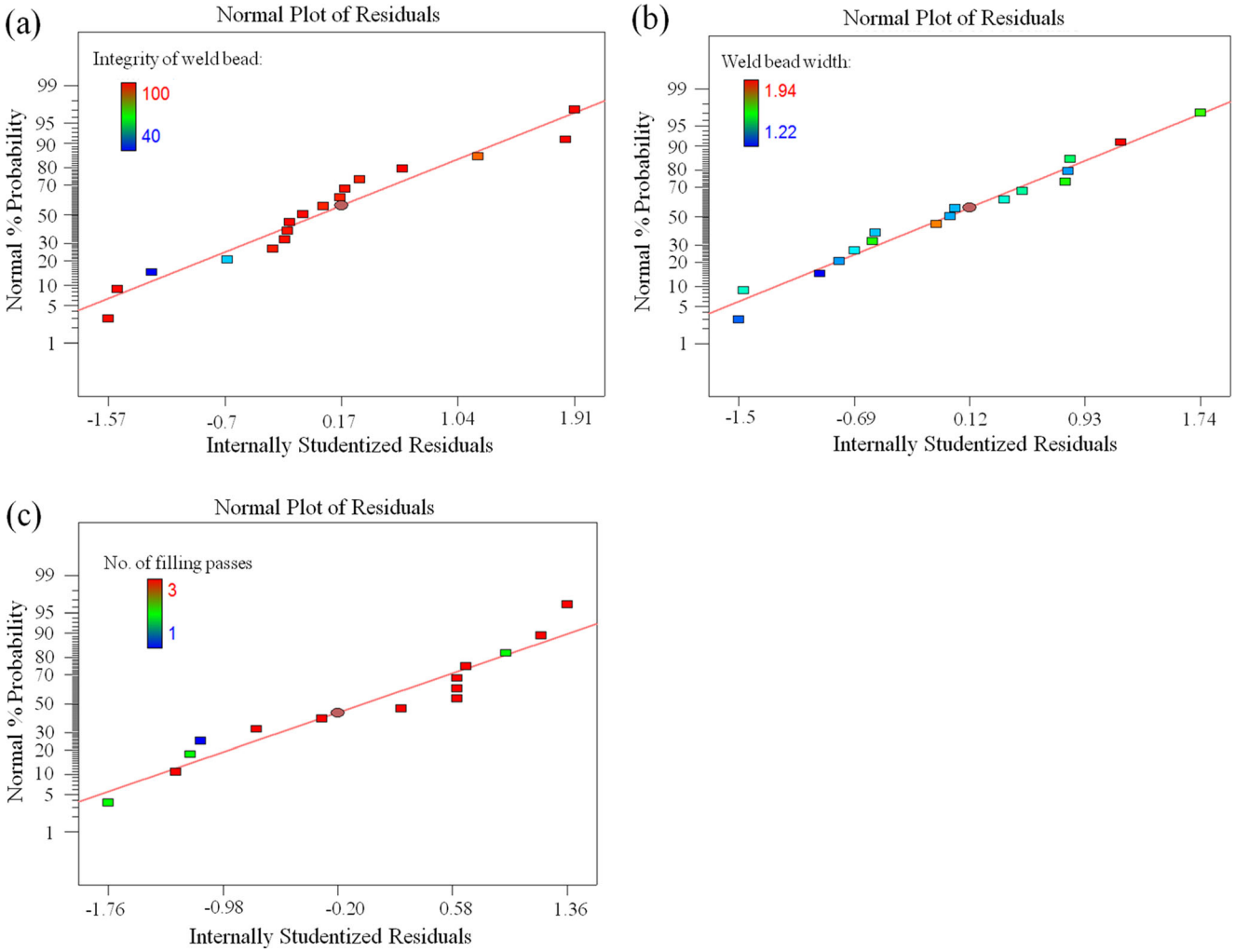

Fig. 8 Residual plots for each model: **a** weld bead integrity model; **b** weld bead width model; and **c** number of filling passes model

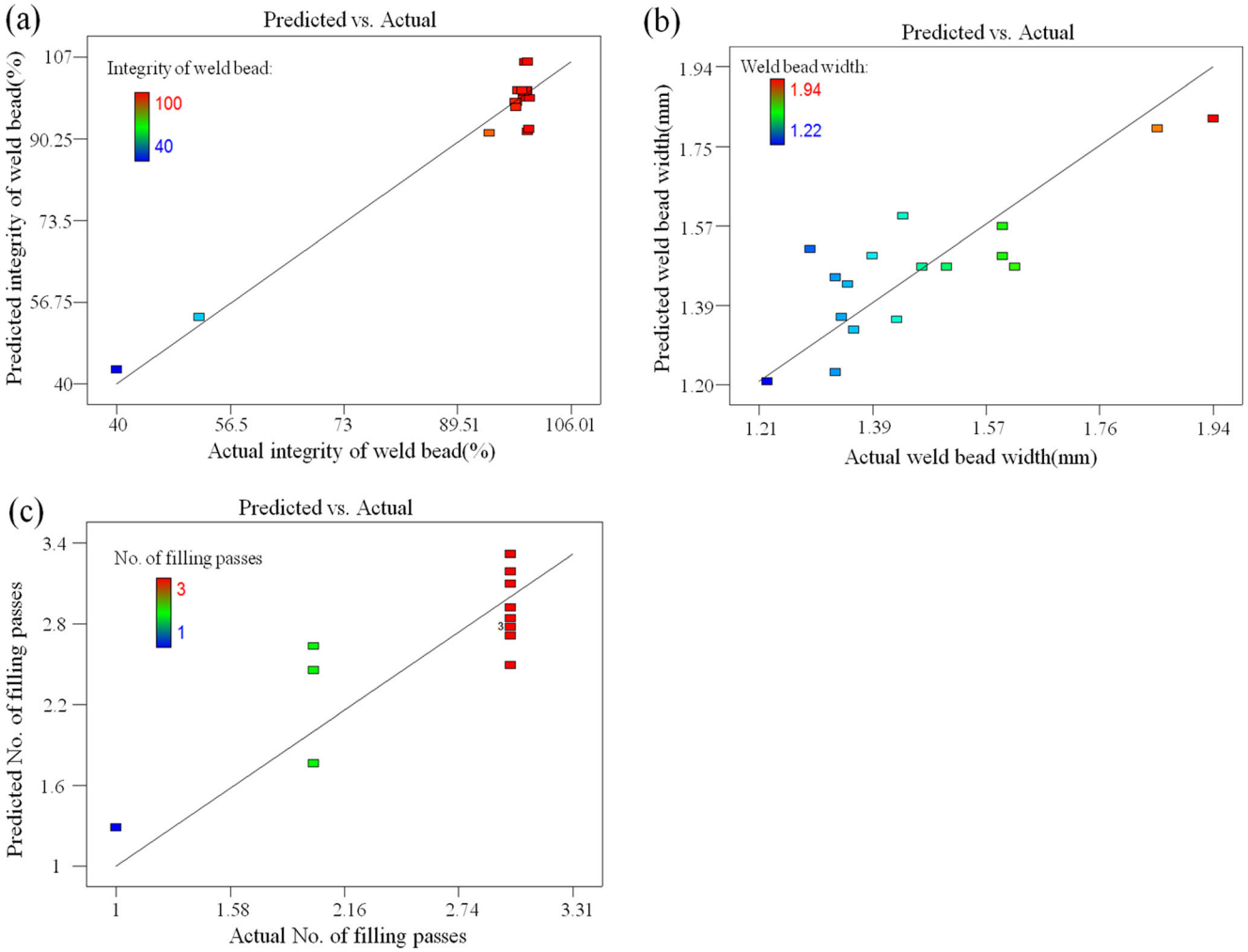

Fig. 9 Comparison of fitted values with measured values for each model: **a** weld bead integrity; **b** weld bead width; **c** number of filling passes

slight influence on the weld bead integrity. However, the wire feed rate has a direct correlation and a stronger effect, with an increase in the wire feed rate leading to a marked increase in the weld bead integrity.

The response surfaces for the weld bead integrity model are shown in Fig. 11. The relationship between the laser power and welding speed is shown in Fig. 11a. It indicates that the weld integrity will be maximised with a high laser power and a low welding speed. However, the weld integrity drops dramatically with a high laser power and a high welding speed. This may be because the high welding speed results in less filler wire being deposited in the groove during each weld pass, and the deposited metal may shrink significantly because there is less weld metal available to resist the shrinkage. Shrinkage in the fusion zone makes it progressively more difficult for the filler wire to fill the groove properly in the following welding passes, and this increases the possibility of generating of lack of fusion or porosity. Furthermore, owing to the high welding speed, the molten filler wire will solidify quickly and this can make it difficult for pores to escape from the molten pool, leading to formation of porosity. Figure 11b presents the relationship between the laser power and the wire feed rate. The

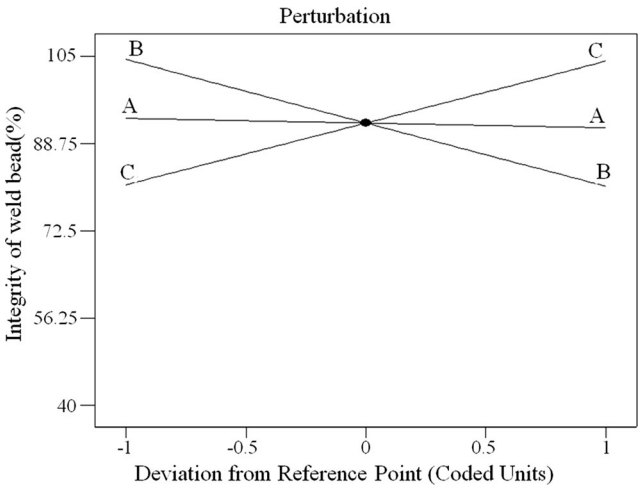

Fig. 10 Perturbation plot showing the effects of all factors on the weld bead integrity, *x*-axis: variables vary at different levels. *A* is laser power, *B* is welding speed and *C* is wire feed rate

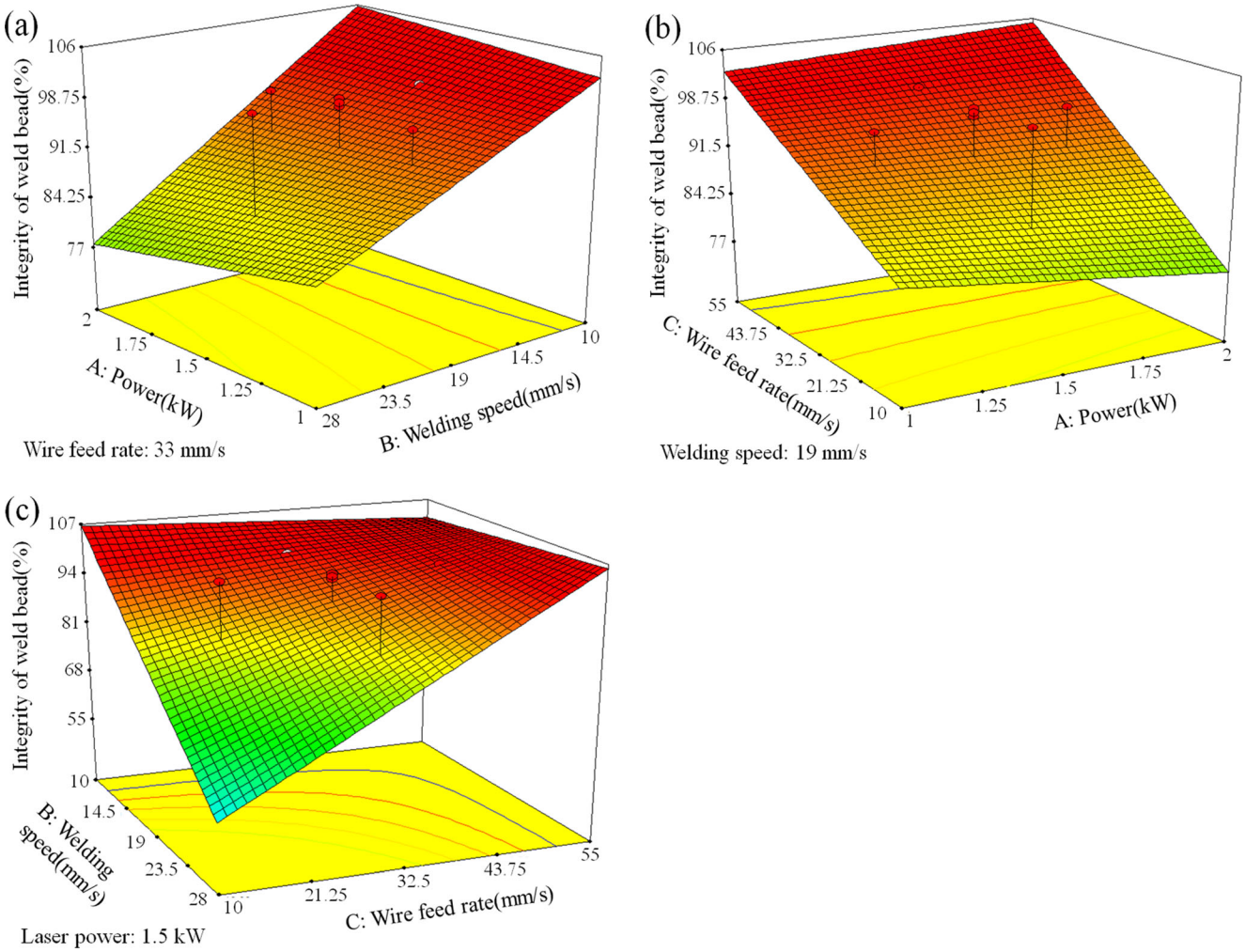

Fig. 11 Response surface graphs for the integrity of the weld bead: **a** laser power-welding speed; **b** laser power-wire feed rate; **c** welding speed-wire feed rate. *A* is the laser power, *B* is the welding speed and *C* is the wire feed rate

integrity of the weld bead can be improved by increasing the laser power and the wire feed rate simultaneously. The higher feed rate will enable the molten filler wire to fill the groove completely when employing a higher laser power, which will help in avoiding lack of fusion. In addition, the higher deposition rate for each pass will assist in resisting shrinkage of the weld bead, which will lead to less distortion and make it easier to deposit filler material in the following weld passes, thereby enabling the groove to be filled successfully. The relationship between the welding speed and the wire feed rate is shown in Fig. 11c. The weld bead integrity is not strongly dependent on the wire feed rate and the welding speed when high values of these parameters are employed in combination. However, the weld bead integrity drops dramatically when higher welding speeds are used in combination with a low wire feed rate. This may because that the combination of a high welding speed and low wire feed rate reduces the cross-sectional area of material that is deposited in each welding pass, which means less material is available to resist the shrinkage in the vicinity of the groove. It then becomes more difficult to add the filler material successfully in later weld passes.

4.4.2 Effects of welding parameters on the weld bead width

Figure 12 is a perturbation plot that illustrates the effect of welding parameters on the weld bead width. It is evident that both the laser power and the wire feed rate demonstrate a direct correction with the weld bead width. An increase in either the laser power or the wire feed rate at a certain welding speed will lead to corresponding increases in the heat input or the quantity of material that is deposited per unit length of weld, respectively, and both of these will translate to an increase in the bead width. The welding speed, however, has a strong inverse correlation with the bead width. An increase in the welding speed reduces the heat input of the welding process, which generally results in a reduction in the size of the molten pool, and hence a reduction in the bead width.

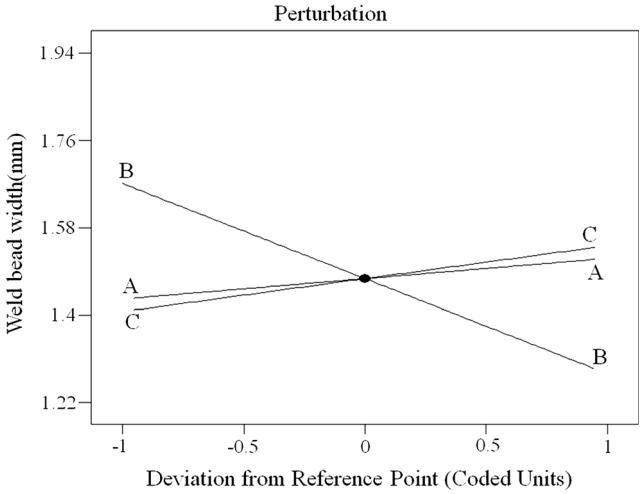

Fig. 12 Perturbation plot showing the effects of all factors on the weld bead width, *x*-axis: variables vary at different levels. *A* is the laser power, *B* is the welding speed and *C* is the wire feed rate

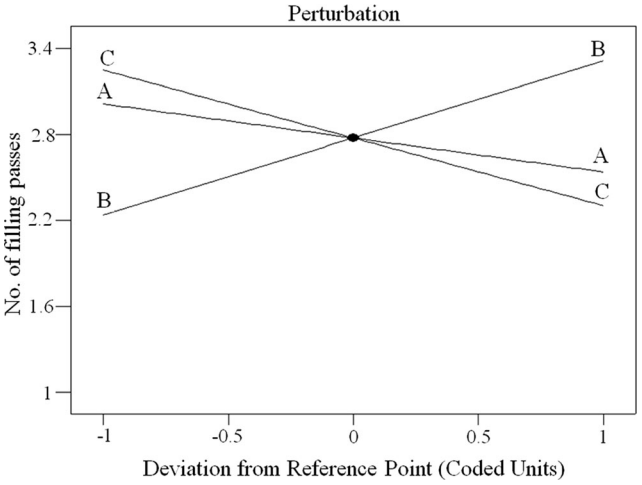

Fig. 14 Perturbation plot showing the effects of all factors on the number of filling passes, *x*-axis: variables vary at different levels. *A* is the laser power, *B* is the welding speed and *C* is the wire feed rate

The response surfaces for the weld bead width model are shown in Fig. 13. From the relationship between the laser power and the welding speed in Fig. 13a, it can be deduced that the combination of a high laser power and a low welding

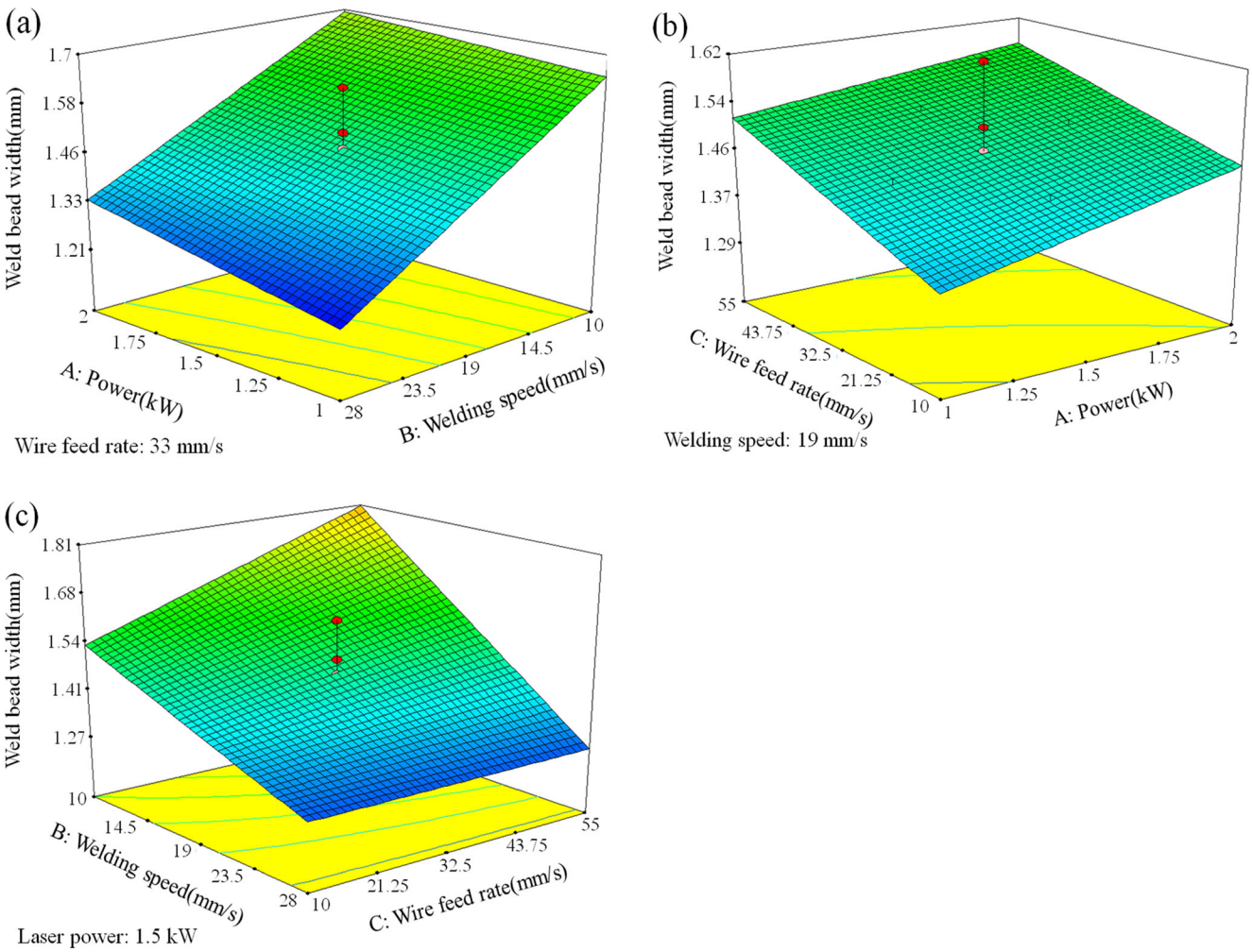

Fig. 13 Response surface graphs for the width of the weld bead: **a** laser power-welding speed; **b** laser power-wire feed rate; **c** welding speed-wire feed rate. *A* is the laser power, *B* is the welding speed and *C* is the wire feed rate

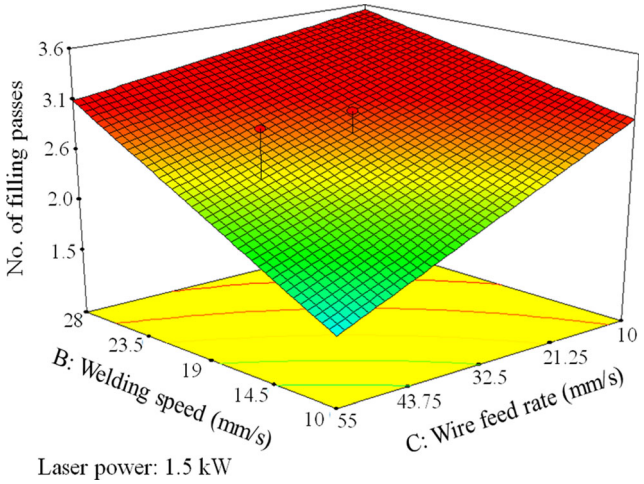

Fig. 15 Response surface graphs for the number of filling passes

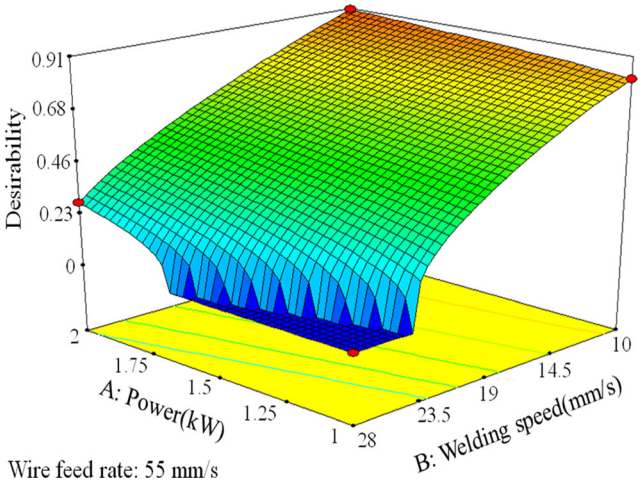

Fig. 16 Desirability shape function for ultra-narrow gap laser welding (wire feed rate 55 mm/s (3.3 m/min))

speed will increase the weld bead width. Conversely, the choice of a lower laser power and a high welding speed will lead to a dramatic reduction in the weld bead width because this combination of parameters will lead to a low heat input. The relationship between the laser power and the wire feed rate is shown in Fig. 13b. It can be seen that the weld bead width increases with increases in both the laser power and the wire feed rate. As was mentioned earlier, increasing either the heat input or the cross-sectional area of the weld bead will lead to the production of larger weld beads and higher bead widths. Figure 13c presents the relationship between the welding speed and the wire feed rate. It can be seen that reductions in the welding speed and increases in the wire feed rate also increase the weld bead width. Here, the effect of the welding speed can also be explained in terms of its influence on the weld heat input. Conversely, increases in the welding speed and reductions in the wire feed rate will lead to dramatic reductions in the weld bead width.

4.4.3 Effects of welding parameters on the number of filling passes

The perturbation plot for the effects of welding parameters on the number of filling passes is shown in Fig. 14. It can be seen that the laser power and the wire feed rate are inversely correlated with the number of filling passes, whilst the welding speed has a direct correlation with the number of filling passes. The correlation between laser power and the number of filling passes is weaker than that for the wire feed rate. Consequently, increasing the wire feed rate and decreasing the welding speed would constitute an effective strategy for reducing the number of filling passes that is required to complete the welded joint.

The response surface graph in Fig. 15 indicates that the number of filling passes drops with increases in the wire feed rate and also with reductions in the welding speed. Increases in the wire feed rate and reductions in the welding speed lead to an increase in the volume of filler material that is deposited per unit length and, consequently, the average height of each filling pass. This will mean that a weld of a given thickness will be completed in fewer passes. Increasing the wire deposition rate will also lead to reduced joint completion times.

4.5 Welding parameter optimisation and validation

4.5.1 Multiple-objective optimisation

In order to obtain high quality narrow gap laser welded joints, the welding parameters need to be optimised. There are many welding parameters involved in the ultra-narrow gap laser welding process, and there are interactions between the effects that these welding parameters have on weld quality. That means that taking measures to improve one response may deteriorate another. In such cases, a multiple variable optimisation may be employed. Such an approach can be advantageous because it can identify the working range for each of the variables in order to satisfy the specified optimisation criteria

Table 9 Multiple-objective optimisation results

Laser power (kW)	Welding speed (mm/s)	Wire feed rate (mm/s)	Weld bead integrity (%)	Weld bead width (mm)	No. of filling passes	Desirability (%)
2	10 (0.6 m/min)[a]	55 (3.3 m/min)[a]	100	1.82	1	90.5

[a] Denotes converted unit of welding speed and wire feed rate to m/min

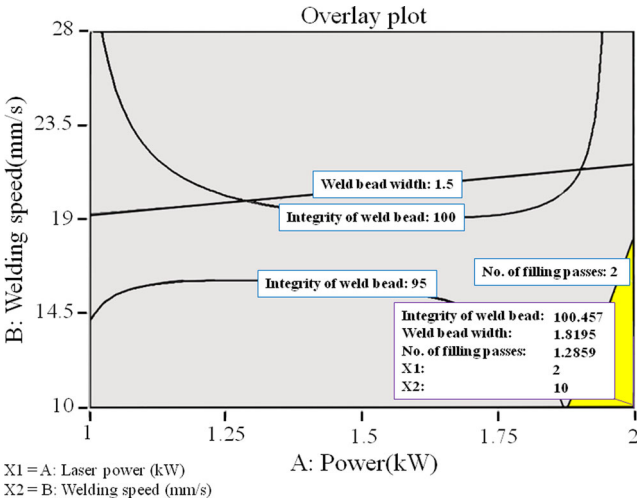

Fig. 17 Optimum welding parameters overlay plot considering all constraints for all variables

for all of the responses simultaneously. Statistical optimisation is achieved through a dimensionless objective function called "desirability". The desirability function approach involves transforming each response, Y_i, into a dimensionless value, d_i, between 0 and 1 [9, 24]. A higher d_i value implies that the corresponding response value is more desirable. The individual desirability of each response can be calculated using Eqs. (8) and (9) [9, 32]. The shape of the desirability function can be changed for each goal through the weight field wt_i. Weights are used to give more emphasis to the upper/lower bounds or to emphasise the target value. Importance varies from the least important value of 1, indicated by (+), to the most important value of 5, indicated by (+++++) [32].

For the goal of maximum, the desirability can be defined by

$$d_i = \begin{cases} 0, & Y_i \le \mathrm{Low}_i \\ \left(\dfrac{Y_i - \mathrm{Low}_i}{\mathrm{High}_i - \mathrm{Low}_i}\right)^{wt_i}, & \mathrm{Low}_i < Y_i < \mathrm{High}_i \\ 1, & Y_i \ge \mathrm{High}_i \end{cases} \quad (8)$$

For the goal of minimum, the desirability can be defined by

$$d_i = \begin{cases} 1, & Y_i \le \mathrm{Low}_i \\ \left(\dfrac{\mathrm{High}_i - Y_i}{\mathrm{High}_i - \mathrm{Low}_i}\right)^{wt_i}, & \mathrm{Low}_i < Y_i < \mathrm{High}_i \\ 0, & Y_i \ge \mathrm{High}_i \end{cases} \quad (9)$$

The final goal of the optimisation is to find a good set of parameters that satisfy all of the goals [9, 32]. Each criterion (maximisation or minimisation) has a specific importance factor according to its influence on the final weld bead quality [9, 29]. This value is specified for each optimisation criterion. In order to satisfy multi-objective optimisation, the desirability function is defined by the geometric mean of all individual desirabilities that range from 0 for the least desirable settings to 1 for the most desirable process settings [9, 24]. The function is defined as [9, 24, 32]

$$\delta = \left(\prod_{i=1}^{n} d_i\right)^{\frac{1}{n}} \quad (10)$$

This equation represents the overall desirability function, where δ is the overall desirability, n is the number of responses and d_i is the ith response desirability value. In this work, both numerical and graphical optimisation approaches were used by selecting the desired goals for each factor and response.

4.5.2 Numerical and graphical optimisation

The numerical optimisation approach involved combining the final goals into an overall desirability function. However, each optimisation criterion has a different effect on the final weld bead quality. In such cases, each optimisation criterion can be assigned a different weight according to the degree of influence it has in the process optimisation [9, 29]. In this investigation, the numerical multiple-response optimisation criterion is to obtain maximum weld bead integrity, maximum weld

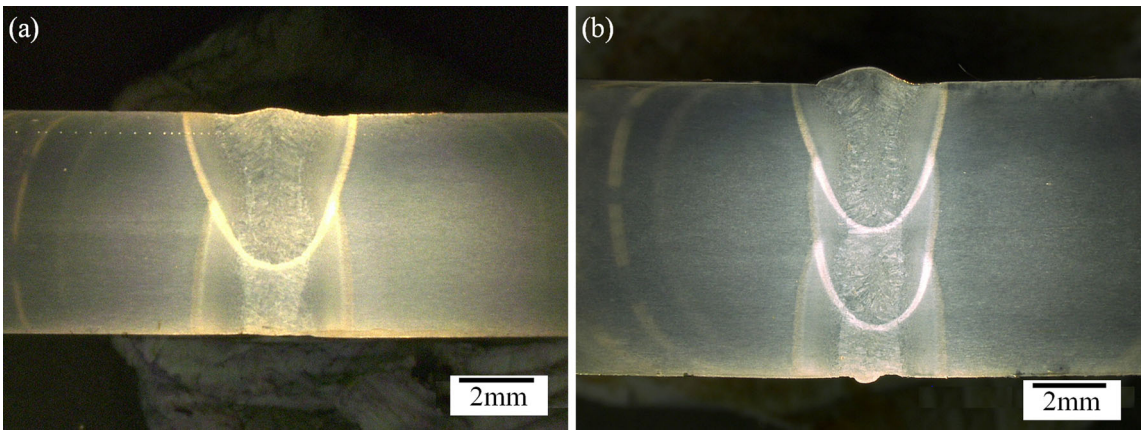

Fig. 18 Cross sections of ultra-narrow gap laser welds in S960 steel: **a** 6 mm thick cross section; **b** 8 mm thick cross section (laser power, 2 kW; welding speed, 0.6 m/min; wire feed rate, 3.3 m/min)

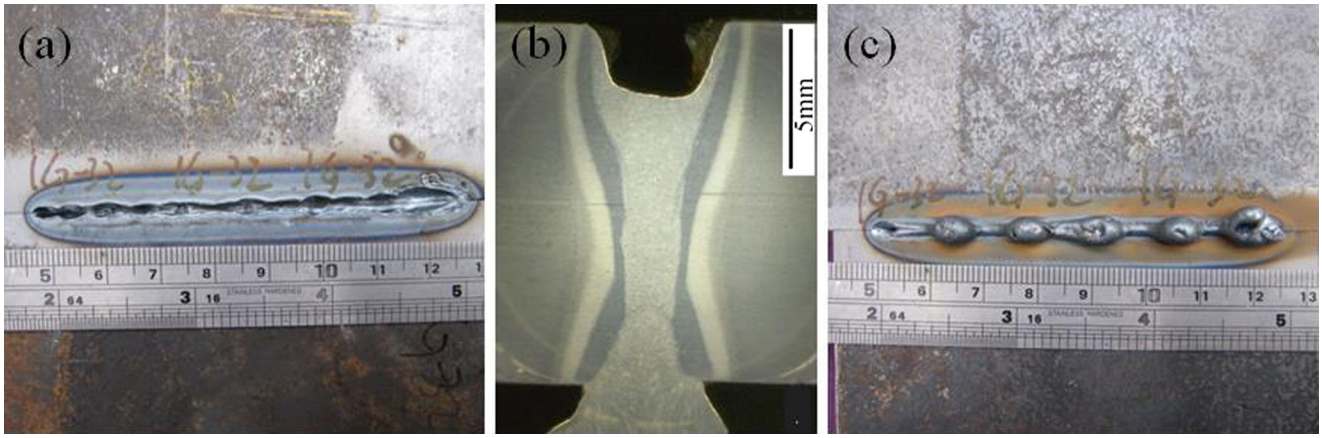

Fig. 19 Typical melt sagging defects for single pass autogenous laser welding of 13 mm thick S700 steel in the flat (1G) position: **a** top weld appearance; **b** weld cross section; **c** underside appearance

bead width in order to improve the weld quality, and the minimum the number of filling passes in order to improve the welding efficiency. The weld bead integrity model was given the highest weight value of 5 (+++++) due to its importance on the final quality of the weld and the mechanical properties of the welded joint. The weld bead width is also important to the mechanical properties of the welded joint, so it was given the second highest weight value of 4 (++++). The number of filling passes was given the weight value of 3 (+++). This criterion was deemed to be of lower importance than obtaining a sound weld.

According to the above optimisation procedure, the details of the most desirable solution and the response values are presented in Table 9. In order to facilitate comparison with arc welding processes in the future, the units for the welding speed and the wire feed rate were converted from millimetre/second to metre/minute. The total desirability value is 90.5 %. The weld bead integrity is 100 %. The weld bead width is 1.82 mm and the number of filling passes is 1. In addition, the desirability shape function (wire feed rate, 55 mm/s (3.3 m/min)) for the ultra-narrow gap laser welding process is shown in Fig. 16. The desirability only has one peak region, and it is obtained by increasing the laser power and decreasing the welding speed.

Only limited sets of optimised welding parameters can be obtained in the numerical optimisation process, so it is not convenient for application in industry. However, in the

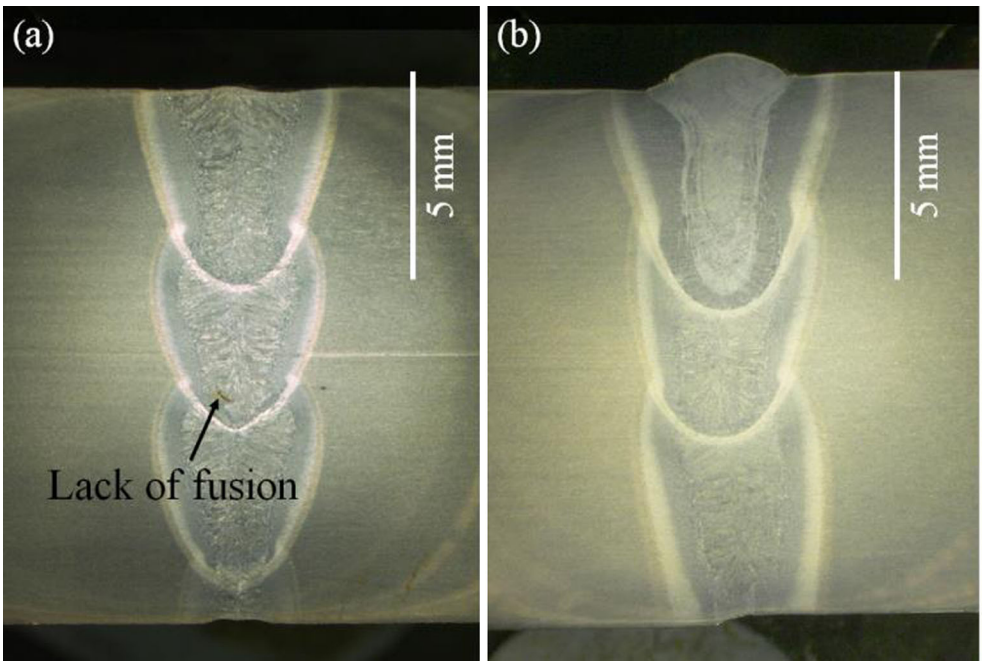

Fig. 20 Cross sections of ultra-narrow gap laser welds in S700 steel: **a** sample welded with parameters (laser power, 2 kW; welding speed, 0.6 m/min; wire feed rate, 3.3 m/min); **b** sample welded with parameters (laser power, 3 kW; welding speed, 0.6 m/min; wire feed rate, 3.3 m/min)

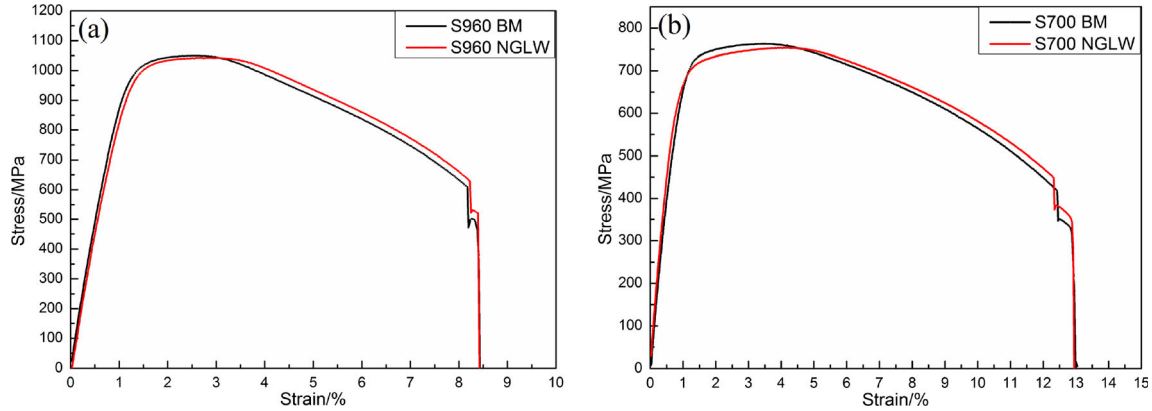

Fig. 21 Representative engineering stress versus engineering strain curves for base material and the ultra-NGLW joints: **a** S960 steel; **b** S700 steel

graphical optimisation process, it is possible to define regions in which the process parameters simultaneously satisfy the different optimisation criteria. The critical responses can be overlayed on a single contour plot, and such a plot is referred to as an overlay plot. The graphical optimisation displays the region of feasible response values in the factor space. The results of the graphical optimisation are the overlay plots, which are quite convenient for rapid application in industry when choosing the values of the welding parameters [9, 29]. The maximum and minimum limits for the optimisation constraints for the graphical optimisation were specified according to the numerical optimisation results: i.e. integrity of the weld bead ≥95 %, width of the weld bead ≥1.5 and number of filling passes ≤2. The overlay plot for all the models according to the optimisation constraints is shown in Fig. 17. The yellow area highlights the region comprising optimum conditions, for which all criteria are satisfied simultaneously. According in Fig. 16, a higher laser power and a lower welding speed provide the optimum conditions for each individual constraint. The intersection area for all constraints is consistent with the numerical optimisation results in Fig. 16.

4.5.3 Validation of the optimised welding parameters

New sets of welding experiments based on the optimised welding parameters, as obtained from the maximum desirability solution in Table 9, were carried out to evaluate the reliability of the modelling work. The 8-mm-thick S960 steel was machined with the same width of groove (1.2 mm) for ultra-narrow gap laser welding. Figure 18 shows the weld cross sections for the 6-mm-thick and 8-mm-thick S960 steel welds. One filling pass was required for ultra-narrow gap laser welding of 6 mm thick S960 steel and two filling passes were required for ultra-narrow gap laser welding of 8 mm thick S960 steel. There was no evidence of lack of fusion or porosity.

It was found that melt pool sagging was one of the characteristics of single pass autogenous laser welding of 13 mm thick S700 steel in the flat (1G) position, as shown in Fig. 19. To solve this melt sagging problem, an attempt was made to transfer the above-mentioned optimised welding parameters (laser power, 2 kW; welding speed, 0.6 m/min; wire feed rate, 3.3 m/min) to the welding of 13 mm thick S700 steel plates using the narrow gap laser welding (NGLW) technique.

Some lack of fusion was found between the two filling passes when using the above optimised welding parameters, as can be seen in Fig. 20a. This may because the input energy was absorbed primarily by the side walls. The laser power was then increased to 3 kW, with the welding speed and wire feed rate unchanged, to weld the 13-mm-thick S700 steel plates. Figure 20b shows the weld cross sections for the 13-mm-thick S700 steel weld made with a laser power of 3 kW. Three filling passes were required for ultra-narrow gap laser welding of 13 mm thick S700 steel plates. There was no evidence of lack of fusion or porosity. In addition, the melt sagging

Table 10 Tensile properties for the base material and the ultra-NGLW specimens

Test specimen	Yield strength (MPa)	Tensile strength (MPa)	Elongation (%)
Base S960 (8 mm)	1026±7	1035±11	8.5±0.3
NGLW S960 (8 mm)	1019±8	1040±11	8.3±0.3
Base S700 (13 mm)	724±7	763±5	12.9±0.8
NGLW S700 (13 mm)	714±5	748±5	12.8±0.4

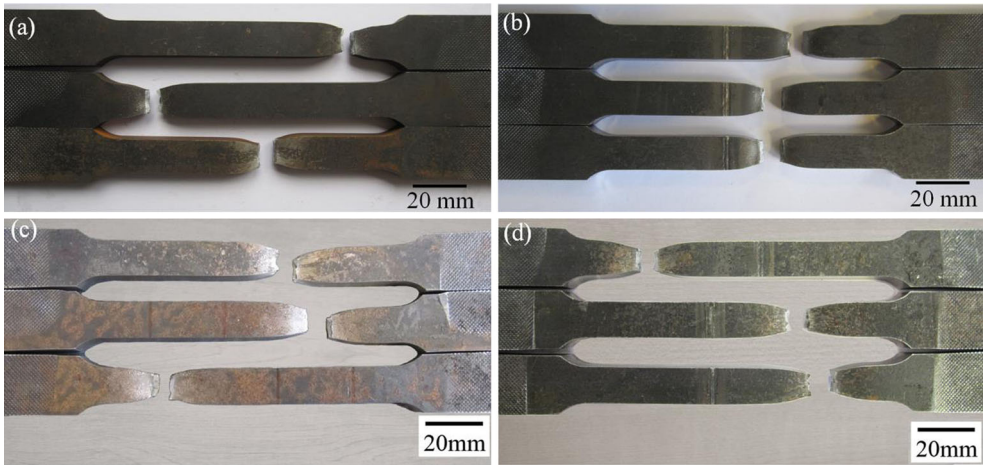

Fig. 22 Fracture locations for the tensile test specimens: **a** base S960 steel; **b** NGLW S960 samples; **c** base S700 steel; **d** NGLW S700 samples

problem was resolved by using this multi-pass ultra-narrow gap laser welding technique to weld this 13 mm thick S700 steel.

4.5.4 Tensile properties

Tensile testing was carried out on the as-received 8-mm-thick S960 and 13-mm-thick S700 base materials and the optimised narrow gap laser welded samples. Typical engineering stress–strain plots for the base materials and the narrow gap laser welded (NGLW) steel joints are shown in Fig. 21. It can be seen that both of the NGLW steel joints present almost the same tensile properties as the base material. The tensile test results are summarised in Table 10, which lists average values and standard deviations. The yield strength (YS), ultimate tensile strength (UTS) and apparent elongation for the NGLW S960 steel samples were found to be 1019 MPa, 1040 MPa and 8.3 %, respectively. The YS, UTS and apparent elongation of the NGLW S960 steel samples were observed to be the same as those for the base S960 steel, which had a YS of 1026 MPa, a UTS of 1035 MPa and an apparent elongation of 8.5 %. The YS, UTS and apparent elongation for the NGLW S700 steel samples were found to be 714 MPa, 748 MPa and 12.8 %, respectively. The YS, UTS and apparent elongation of the base S700 steel were 724 MPa, 763 MPa and 12.9 %, respectively. All tensile failures for the welded specimens were in the base material well away from the weld, as is shown in Fig. 22. This means that the optimised NGLW specimens retained good tensile properties. It should be noted, however, that the elongations measured in this work do not capture the behaviour of the weld region itself very effectively, since the elongations were averaged across the weld zone and the parent material. While these preliminary results are encouraging, further work would be required in order to obtain a more detailed assessment of the mechanical properties across the welded joints.

5 Conclusions

The following conclusions can be drawn from this investigation:

(1) Ultra-narrow gap laser welding was successfully carried out on 6 and 8 mm thick S960 and 13 mm thick S700 high strength steel plates using a relatively moderate laser power (2–3 kW) and a narrow (1.2–1.4 mm) parallel groove.
(2) The multi-pass ultra-narrow gap laser welding technique provides an alternative solution to solving the melt sagging problem when welding thick section materials.
(3) From the predictions of the statistical model, it was found that the weld quality and the welding efficiency can be improved through increasing the laser power and the wire feed rate, and reducing the welding speed.
(4) The optimised welding parameters were successfully transferred to the welding of 8 mm thick S960 steel with two filling passes, and to the welding of 13 mm thick S700 steel with three filling passes.
(5) The tensile properties of the optimised narrow gap laser welded specimens matched those of the base material, with all welded specimens failing in the BM.

Acknowledgments The authors acknowledge the financial support of this work by Tata Steel and The University of Manchester scholarship for the funding of the research. The authors are grateful to Mr Damian Crosby, Dr. Xiansheng Shen and Dr. Yanfeng Du for assistance with the laser welding experiments.

References

1. Onoro J, Ranninger C (1997) Fatigue behaviour of laser welds of high-strength low-alloy steels. J Mater Process Technol 68(1):68–70. doi:10.1016/S0924-0136(96)02541-1
2. Shi G, Shi Y, Wang Y (2008) Engineering application of ultra-high strength steel structures. Prog Steel Build Struct 10(4):32–38

3. Yang Y, Lee S (1999) A study on the joining strength of laser spot welding for automotive applications. J Mater Process Technol 94(2):151–156. doi:10.1016/S0924-0136(99)00094-1
4. Mohandas T, Reddy GM (1997) A comparison of continuous and pulse current gas tungsten arc welds of an ultra high strength steel. J Mater Process Technol 69(1):222–226. doi:10.1016/S0924-0136(97)00022-8
5. Goodarzi M, Marashi S, Pouranvari M (2009) Dependence of overload performance on weld attributes for resistance spot welded galvanized low carbon steel. J Mater Process Technol 209(9):4379–4384. doi:10.1016/j.jmatprotec.2008.11.017
6. Bai Y, Bai Q (2005) Subsea pipelines and risers. Elsevier, Oxford, UK
7. Guo W, Liu Q, Francis JA, Crowther D, Thompson A, Liu Z, Li L (2015) Comparison of laser welds in thick section S700 high-strength steel manufactured in flat (1G) and horizontal (2G) positions. CIRP Ann Manuf Technol 64(1):197–200. doi:10.1016/j.cirp.2015.04.070
8. Chen H-C, Pinkerton AJ, Li L, Liu Z, Mistry AT (2011) Gap-free fibre laser welding of Zn-coated steel on Al alloy for light-weight automotive applications. Mater Des 32(2):495–504. doi:10.1016/j.matdes.2010.08.034
9. Elmesalamy A, Li L, Francis J, Sezer H (2013) Understanding the process parameter interactions in multiple-pass ultra-narrow-gap laser welding of thick-section stainless steels. Int J Adv Manuf Technol 68(1–4):1–17. doi:10.1007/s00170-013-4739-x
10. Kristensen JK (2009) Laser and hybrid laser-GMA welding of structural steels a challenge to research and industry for two decades. Trends in Welding Research 2008: Proceedings of the 8th International Conference, pp 645 – 651
11. Bachmann M, Avilov V, Gumenyuk A, Rethmeier M (2014) Experimental and numerical investigation of an electromagnetic weld pool support system for high power laser beam welding of austenitic stainless steel. J Mater Process Technol 214(3):578–591. doi:10.1016/j.jmatprotec.2013.11.013
12. Bachmann M, Avilov V, Gumenyuk A, Rethmeier M (2014) Experimental and numerical investigation of an electromagnetic weld pool control for laser beam welding. Phys Procedia 56:515–524. doi:10.1016/j.phpro.2014.08.006
13. Zhang X, Ashida E, Tarasawa S, Anma Y, Okada M, Katayama S, Mizutani M (2011) Welding of thick stainless steel plates up to 50 mm with high brightness lasers. J Laser Appl 23(2):022002. doi:10.2351/1.3567961
14. Elmesalamy A, Francis J, Li L (2014) A comparison of residual stresses in multi pass narrow gap laser welds and gas-tungsten arc welds in AISI 316L stainless steel. Int J Press Vessel Pip 113:49–59. doi:10.1016/j.ijpvp.2013.11.002
15. Li R, Wang T, Wang C, Yan F, Shao X, Hu X, Li J (2014) A study of narrow gap laser welding for thick plates using the multi-layer and multi-pass method. Opt Laser Technol 64:172–183. doi:10.1016/j.optlastec.2014.04.015
16. Sun Z, Salminen A (1997) Current status of laser welding with wire feed. Mater Manuf Process 12(5):759–777. doi:10.1080/10426919708935183
17. Shi H, Zhang K, Xu Z, Huang T, Fan L, Bao W (2014) Applying statistical models optimize the process of multi-pass narrow-gap laser welding with filler wire. Int J Adv Manuf Technol 75(1–4):279–291. doi:10.1007/s00170-014-6159-y
18. Lee H-K, Han H-S, Son K-J, Hong S-B (2006) Optimization of Nd:YAG laser welding parameters for sealing small titanium tube ends. Mater Sci Eng A 415(1):149–155. doi:10.1016/j.msea.2005.09.059
19. Park YW, Rhee S (2008) Process modeling and parameter optimization using neural network and genetic algorithms for aluminum laser welding automation. Int J Adv Manuf Technol 37(9–10):1014–1021. doi:10.1007/s00170-007-1039-3
20. Benyounis K, Olabi A (2008) Optimization of different welding processes using statistical and numerical approaches—a reference guide. Adv Eng Softw 39(6):483–496. doi:10.1016/j.advengsoft.2007.03.012
21. Talaş Ş (2010) The assessment of carbon equivalent formulas in predicting the properties of steel weld metals. Mater Des 31(5):2649–2653. doi:10.1016/j.matdes.2009.11.066
22. Yu YC, Yang SL, Yin Y, Wang CM, Hu XY, Meng XX, Yu SF (2013) Multi-pass laser welding of thick plate with filler wire by using a narrow gap joint configuration. J Mech Sci Technol 27(7):2125–2131. doi:10.1007/s12206-013-0525-9
23. Benyounis K, Olabi A-G, Hashmi M (2008) Multi-response optimization of CO_2 laser-welding process of austenitic stainless steel. Opt Laser Technol 40(1):76–87. doi:10.1016/j.optlastec.2007.03.009
24. Leigh S, Sezer K, Li L, Grafton-Reed C, Cuttell M (2009) Statistical analysis of recast formation in laser drilled acute blind holes in CMSX-4 nickel superalloy. Int J Adv Manuf Technol 43(11–12):1094–1105. doi:10.1007/s00170-008-1789-6
25. Box GE, Wilson K (1951) On the experimental attainment of optimum conditions. J R Stat Soc Ser B 13(1):1–45
26. Montgomery DC (2008) Design and analysis of experiments. Wiley
27. Khuri AI, Cornell JA (1996) Response surfaces: designs and analyses, vol 152. CRC Press, Boca Raton
28. Palani P, Murugan N (2007) Optimization of weld bead geometry for stainless steel claddings deposited by FCAW. J Mater Process Technol 190(1):291–299. doi:10.1016/j.jmatprotec.2007.02.035
29. Reisgen U, Schleser M, Mokrov O, Ahmed E (2012) Statistical modeling of laser welding of DP/TRIP steel sheets. Opt Laser Technol 44(1):92–101. doi:10.1016/j.optlastec.2011.05.025
30. Khan M, Romoli L, Fiaschi M, Dini G, Sarri F (2011) Experimental design approach to the process parameter optimization for laser welding of martensitic stainless steels in a constrained overlap configuration. Opt Laser Technol 43(1):158–172. doi:10.1016/j.optlastec.2010.06.006
31. Khan M, Romoli L, Fiaschi M, Dini G, Sarri F (2012) Multiresponse optimization of laser welding of stainless steels in a constrained fillet joint configuration using RSM. Int J Adv Manuf Technol 62(5–8):587–603. doi:10.1007/s00170-011-3835-z
32. Ruggiero A, Tricarico L, Olabi A, Benyounis K (2011) Weld-bead profile and costs optimisation of the CO_2 dissimilar laser welding process of low carbon steel and austenitic steel AISI316. Opt Laser Technol 43(1):82–90. doi:10.1016/j.optlastec.2010.05.008